Scientific Reports

https://doi.org/10.1038/s41598-026-40396-8

Article in Press

MOV10, a novel immunotherapy and prognostic biomarker, contributes to glioma development by regulating autophagy

Received: 23 June 2025

Accepted: 12 February 2026

Published online: 18 February 2026

Cite this article as: Wang F., Ruan L., Yang W. *et al.* MOV10, a novel immunotherapy and prognostic biomarker, contributes to glioma development by regulating autophagy. *Sci Rep* (2026). https://doi.org/10.1038/s41598-026-40396-8

Feiyu Wang, Linlin Ruan, Wenbin Yang, Yueben Hu, Yangzhong Guo, Xuanxuan Xiong, Dan Liu, Qiaoli Lv & Shuhui Chen

MOV10, a novel immunotherapy and prognostic biomarker, contributes to glioma development by regulating autophagy

Feiyu Wang[c], Linlin Ruan[a, b], Wenbin Yang[b], Yueben Hu[d], Yangzhong Guo[a], Xuanxuan Xiong[b], Dan Liu[b], Qiaoli Lv[a*], Shuhui Chen[a*]

[a]Jiangxi Key Laboratory of oncology(2024SSY06041), JXHC Key Laboratory of Tumour Metastasis, Jiangxi Cancer Hospital & Institute, The Second Affiliated Hospital of Nanchang Medical College, Nanchang, Jiangxi, 330029, P.R. China.

[b]School of pharmacy, Nanchang University, Nanchang 330006, P.R. China

[c]Yichun College, Yichun 336000, P.R. China

[d]Department of Pharmacy, Nanchang People's hospital(Nanchang Third hospital), Nanchang, 330009, P.R. China

[*] Correspondence

lvqiaoli2008@163.com

chenshuhui2008@126.com(Shuhui Chen),

Abstract

Glioblastoma (GBM) is a highly aggressive and lethal brain tumor, and despite conventional treatments, patient prognosis remains poor. Understanding the molecular mechanisms driving GBM and identifying potential therapeutic targets is critical. MOV10, an RNA helicase, is overexpressed in multiple cancers and is considered an oncogene. Our analysis of datasets from TCGA, GEO, and CGGA showed that MOV10 expression is elevated in GBM and strongly negatively correlated with overall survival (OS). Cox regression confirmed MOV10 as an independent prognostic risk factor for GBM.Functional enrichment analysis revealed that MOV10 is involved in immune regulation and tumor progression pathways. We found that MOV10 expression is closely linked to immune infiltration, immune checkpoint expression, and responses to immunotherapy. Immunofluorescence and Transwell assays confirmed that MOV10 knockdown

reduced M2 macrophage migration and invasion in GBM cells. Clinical analysis further validated MOV10 overexpression in GBM tissues.In vitro, MOV10 silencing suppressed GBM cell proliferation, inhibited EMT-like processes, and promoted apoptosis through autophagy modulation. Our findings suggest that MOV10 plays a crucial role in GBM progression and could be a promising molecular target for therapy.

Keywords: glioma, MOV10, immune infiltration, epithelial-mesenchymal transformation, autophagy, apoptosis

Introduction

Gliomas are the most common type of primary malignant tumor in the central nervous system, known for their high recurrence, disability, and mortality rates, as well as a low cure rate [1]. According to WHO, more than 11 million people are diagnosed with gliomas annually [2]. Gliomas are categorized into WHO grades I to IV, based on malignancy level [3], with glioblastoma (GBM) being the most aggressive. GBM patients have a median survival time of just 8 months, with only 3% to 5% of them surviving more than 3 years [4]. The primary reasons for poor prognosis include treatment resistance and tumor recurrence after surgery. The exact mechanisms behind the aggressive growth of gliomas remain unclear [5], making treatment particularly challenging. As a result, there is a pressing need to investigate the biological origins of gliomas, identify potential diagnostic and therapeutic targets, and develop new treatment strategies .

Moloneyleukemiavirus10 (MOV10) protein is a newly discovered factor with broad-spectrum antiretroviral potential. MOV10 proteins belong to RNA helicase superfamily 1 (SF-1) [6, 7]. MOV10 can interact with AGO2 (Argonaute 2) and participate in the metabolism and translation of mRNA [8]. It is a component of the RNA-induced silencing complex (RISC) [9]. MOV10 is a new type of RNA binding protein (RBP) that is highly expressed in cancer cells and is considered to be an oncogene [10]. The expression of MOV10

protein is significantly increased in pancreatic cancer, and as an RBP protein, it improves the proliferation and invasive ability of pancreatic cancer cells [11]. Recent studies have shown that MOV10 can mediate the expression of miRNA-103a-3p (miRNA-382-5p) by binding to circ-DICER1 and then affect the angiogenesis of glioma cells by regulating the PI3K/AKT signalling pathway [12]. The above studies suggest that MOV10 is related to the occurrence and development of gliomas, but the exact role of MOV10 in glioma cells and its effect on prognosis are still unclear.

Gliomas possess a highly immunosuppressive tumor microenvironment (TME), which contributes to immune evasion and promotes the survival of malignant gliomas [13]. Immunotherapy can regulate immune function, reshape the tumor immune microenvironment, activate the immune system [14], and destroy cancer cells. Forms of tumor immunotherapy include cancer vaccines, oncolytic viruses, cell therapy, and immune checkpoint inhibitors [15]. With the rise of immunotherapy, more and more research is focusing on glioma immunotherapy [16]. Studies have shown that MOV10 may act as an innate immune factor against viruses [17, 18] and as an inhibitor of LINE-1 (L1), playing a role in tumor immunity [19]. However, no research has yet directly explored the relationship between MOV10 and glioma immunity. Given the importance of immunotherapy in gliomas and the connection between MOV10 and immune function, understanding the role of MOV10 in glioma immunity is crucial for developing new therapeutic strategies .

In this study, we leveraged three public databases to examine the differences in MOV10 expression between normal and glioma tissues. We generated overall survival (OS) curves based on factors such as MOV10 expression, tumor grade, age, IDH mutations, and 1p/19q co-deletion, and built a Cox regression model incorporating multiple clinical factors. Furthermore, we explored the relationship between MOV10 and immune cell infiltration, as well as its role in immunotherapy. Experimental validation demonstrated the influence of MOV10 on M2 macrophages in gliomas. We

then analyzed the functional enrichment of MOV10 and examined its underlying molecular mechanisms in regulating the proliferation, migration, invasion, autophagy, and apoptosis of T98G and U251 cells. This study aims to provide a theoretical foundation for the early prevention, treatment, and clinical diagnosis of gliomas.

Materials and Methods

Information Collection

We obtained glioma transcriptome data including LGG (low-grade glioma) and GBM (glioblastoma) from the UCSC database. The LGG dataset contains 529 tumor patient samples, and the GBM dataset contains 5 normal samples and 168 tumor patient samples. The data are provided in FPKM format and have been log2(x+1) transformed. In addition, we downloaded clinical data and MOV10 gene expression data of 693 glioma patients from CGGA (Chinese Glioma Genome Atlas). We also retrieved another set of glioma transcriptome data from the CGGA database, which contains 325 glioma samples. This dataset is in raw count format, and we standardized and log2-transformed it, removing all missing data points. The samples in all datasets represent patients of different ages and genders. All data use was approved by the patients with written informed consent and complied with relevant ethical standards and laws and regulations.

Differential expression of MOV10 in cancer

The GEPIA database (http://gepia2.cancer-pku.cn) is an online platform that provides RNA transcriptome data of 33 cancer types from the TCGA database. This tool can analyze mRNA expression levels in tumor and normal tissue samples and provide visualization results. We used GEPIA to explore the expression of the MOV10 gene in 33 cancers in the TCGA database.

Clinical model analysis

We used the R package "survminer" to analyze the survival data of glioma

patients in the TCGA and CGGA databases. We performed Cox regression analysis and used the receiver operating characteristic (ROC) curve to evaluate the prognostic significance of MOV10 expression in glioma patients. In addition, we applied multivariate logistic regression to classify the risk level of patients in the CGGA data and provide a risk score for each patient. With the help of the "regplot" and "rms" R packages, we created a nomogram for predicting the prognosis of glioma patients. The nomogram included clinical factors such as MOV10 expression, age, sex, PFS type, tumor grade, IDH mutation, and 1p/19q co-deletion, and was calibrated using 1-year, 3-year, and 5-year scores to evaluate its predictive accuracy. According to the median expression level of the MOV10 gene, the patients were divided into high-expression group and low-expression group, and their overall survival rate and the difference in MOV10 expression compared with other clinical subgroups were further analyzed. The “ggplot2” package in RStudio was used for data visualization to clearly and intuitively present the survival curves and gene expression differences.

GO, KEGG and GSEA analysis

The cBioPortal provides comprehensive genomic data from various cancer research projects, including datasets from TCGA, the International Cancer Genome Consortium (ICGC), and others. We leveraged the TCGA Cell 2013 dataset, consisting of 577 glioblastoma (GBM) transcriptomes, to identify genes associated with MOV10. Using R packages "clusterProfiler" and "enrichplot," we conducted GO and KEGG functional enrichment analyses on these associated genes, and visualized the results with "ggplot2." We also extracted TCGA-Glioma data from the TCGA database using the "dplyr" and "tibble" R packages. After merging the datasets, we divided samples into high- and low-expression groups based on MOV10 expression and performed differential expression analysis (DEGs) with the criteria of $|\log2(FC)| > 1.0$ and p-value < 0.05. From MSigDB, we downloaded the "h.all.v2024.1.Hs.symbols"

gene set in GMT format and carried out GSEA analysis using "fgsea," "GSEABase," and "GSVA" R packages. Clusters with a p-value < 0.05 and FDR < 0.25 were considered statistically significant, and select clusters ranked high according to normalized enrichment score (NES) to further investigate the biological functions of the top six pathways in high and low MOV10 expression groups.

Immunity Analysis

We used the "estimate" package to assign scores to glioma patient samples and explored the relationship between MOV10 expression and stromal and immune cell scores through correlation analysis. Survival outcomes were also analyzed across different score groups. Additionally, we applied the CIBERSORT algorithm to assess the correlation between MOV10 expression and immune cells in gliomas, followed by validation with the xCell immune algorithm. We further used the TIDE (Tumor Immune Dysfunction and Exclusion) algorithm to evaluate MOV10's role in immune evasion(http://tide.dfci.harvard.edu), which can partially predict whether patients will respond to immune checkpoint inhibitors, such as PD-1 or CTLA-4 inhibitors. This data was normalized for consistency. Finally, we analyzed the correlation and differences between MOV10 and immune checkpoints, as well as immune-related genes, using glioma data from the TCGA database. This was accomplished through the R packages "corrplot" and "PerformanceAnalytics." The immune checkpoints studied were primarily sourced from literature and prominent immune checkpoints listed on GeneCards (https://www.genecards.org).Using the TCGA-GBM RNA-seq dataset, samples were divided into MOV10-high and MOV10-low groups by the median MOV10 expression. Two T-cell exhaustion subtype signatures (Progenitor_Tex and Terminal_Tex) were collected from published studies. ssGSEA scores for each signature were calculated with the GSVA R package, and the Terminal_Tex and Progenitor_Tex scores were compared within the

MOV10-high group using a paired Wilcoxon test.

Clinical samples and study approval

For expression analysis, all fresh glioma tumour samples were obtained from patients who had histologically confirmed glioma, and normal specimens were collected from patients who underwent brain tissue resection for craniocerebral injury at the Jiangxi Subcentre of the National Clinical Research Center for Cancer (Jiangxi Cancer Hospital Biospecimen Repository). After surgical resection, these samples were rinsed with PBS and preserved in liquid nitrogen for subsequent analysis. None of these patients received preoperative chemotherapy or radiotherapy prior to the study. All experimental protocols were approved by the Ethics Committee of Jiangxi Cancer Hospital (No. 2020ky008), and each enrolled patient provided written informed consent.

Cell lines and cell culture

Glioma cell lines used in the experiments, including the glioma cell lines U87, U251, and T98G and normal cells (HEB), were purchased from the AoYin Cell Center. The cells were cultivated in high-glucose Dulbecco's modified Eagle's medium (DMEM, HyClone, United States) supplemented with 10% FBS (FBS, GIBCO, Carlsbad, California, United States) and 1% penicillin–streptomycin and maintained in a humidified incubator with 5% CO2 at 37 °C. These cell lines tested negative for mycoplasma contamination.

Macrophage generation and differentiation

THP-1 cells (ATCC, catalog number: TIB-202) were cultured in RPMI-1640 medium (Gibco, 11875-093) containing 10% fetal bovine serum-FBS (Gibco, 10099-141) and 1% penicillin-streptomycin mixture (Gibco, 15140-122) and maintained at 37 °C in a 5% CO_2 incubator. The medium was changed and

cells were passaged every 2–3 days, ensuring they were in logarithmic growth phase before the experiment. To obtain M0 macrophages, THP-1 cells were seeded in culture plates and treated with 100 ng/mL PMA (Sigma-Aldrich, P8139) for 24 h, followed by replacement with fresh intact medium and a 24 h recovery period.

Cell transfection

Small interfering RNAs (siRNAs) targeting MOV10 and scramble siRNA were purchased from RiboBio (Guangzhou, China). Glioma cells were plated at 40%-50% confluency in 6-well plates. After 12 h for cell adhesion, transfection was carried out using Lipofectamine® RNAiMAX Transfection Reagent (Invitrogen, Carlsbad, California, United States) at a final concentration of 100 nM in accordance with the instructions. In addition, the growth medium was without antibiotics. The sequences of the siRNAs are as follows: siMOV10_001: AGACTCGGTCAGGTTCTT; siMOV10_002: GTGGATCGAGAACGCTTCT

RNA isolation and reverse transcription (RT)-PCR assay

TRIzol reagent (Takara, Dalian, China) was utilized to extract total RNA from glioma cells and tissues. The collected RNA was subsequently dissolved in 10 µl of DEPC-treated water, and the RNA concentration and purity were detected at the 260/280 nm ratio. Then, reverse transcription was performed using the PrimeScript™ RT reagent Kit with gDNA Eraser (Takara, Dalian, China) to produce complementary DNA (cDNA). Quantitative real-time polymerase chain reaction (qRT–PCR) was performed using TB Green® Premix Ex Taq™ II (Takara, Dalian, China) on a Bio-Rad CFX96 Touch sequence detection system (Bio-Rad Laboratories Inc.) according to the manufacturer's instructions. GAPDH was used as an endogenous control, and the target gene expression level was calculated by means of the $2^{-\Delta\Delta CT}$ method. Each experiment was performed in triplicate, and each sample was

analysed in two parallel wells. The primers for MOV10 were F: 5’-GGGGACTGGACATGGAGACA-3’; and R: 5’-GGGTCCCAAAGCTGATCTTGA-3’. The primers for GAPDH were F: 5’-CCCATCACCATCTTCCAGGAG-3’ and R: 5’-GTTGTCATGGATGACCTTGGC-3’.

Western blot assays

Cells were transfected with siRNAs to transiently knockdown target genes, and 72 h after transfection, cells were harvested and lysed in RIPA buffer (Beyotime, Shanghai, China) containing 1% protease inhibitor cocktails (Beyotime, Shanghai, China). The lysate was centrifuged at 13000 rcf 4 °C for 15 min to obtain the supernatants, and the protein concentration of the supernatant extract was determined by a BCA protein assay kit (TIANGEN, Beijing, China). The supernatants were denatured with 6× loading buffer (TransGen Biotech, Beijing, China) and heated at 100 °C for 10 min. Next, the samples were separated by SDS–PAGE and transferred onto polyvinylidene fluoride membranes. The membranes were then blocked with 5% skimmed milk for 2 h and incubated with primary antibodies at 4 °C overnight. Then, the membranes were subsequently reprobed with species-matched secondary antibodies for 2 h. Antibodies were purchased from CST Biotechnology (Boston, Massachusetts, United States). Bands on immunoblots were detected with an ECL kit (YaMei, Shanghai, China) and visualized on a ChemiDoc Touch Imaging System (ChemiDoc XRS+). β-Actin was used as an internal control.

Transwell assay and wound healing assays

Cell invasion ability was evaluated using Transwell chambers (Corning, Tewksbury, Massachusetts, United States) with a membrane pore size of 8 μm. First, Matrigel was diluted in serum-free medium at 1:9 with 70 μl of Matrigel dilution supplemented into the upper layer of the transwell

membrane and incubated for 2-3 h to polymerize the Matrigel. Then, the cells were dissociated with pancreatin and resuspended in serum-free medium until the final cell density reached 1.5× 10^5 cells/ml. Next, the remaining liquid was removed from the top side of the chamber, and 200 µl of cell suspension was seeded in the upper chambers, whereas 700 µl medium containing 10% FBS was subsequently added to the lower chamber as an attractant. After 48 h of cultivation, cells on the upper side of the membrane were wiped off with cotton swabs. Cells that invaded to the lower side of the membrane were then subjected to fixation with paraformaldehyde for 30 min followed by staining with 0.1% crystal violet overnight. Thereafter, each transwell chamber was gently washed with PBS, air dried and photographed under an inverted microscope. For wound-healing assays, cells were transfected in a six-well plate for 48 h with a cell density of 80%-90%. Next, the cell monolayer was scratched with a 200 µl pipette tip and subsequently washed with PBS solution and replaced with high glucose DMEM containing 2% serum medium to continue culturing the cells. Finally, images were captured under a light microscope at 0 h and 24 h after scratching.

Cell proliferation and colony formation assays

The effects of gene manipulation were evaluated using MTS and colony formation assays to explore the proliferation potential of GBM cells after transfection with MOV10 siRNA for 48 h. Briefly, cells were seeded in 96-well plates at a density of 2000 cells per well and measured every 24 h for 5 continuous days at indicated times. According to the manufacturer's protocol, MTS solution (Cell Titer 96 aqueous one solution reagent, Promega, Madison, Wisconsin, United States) and serum-free medium were mixed at a ratio of 1:9. Subsequently, the mixture was added to a plate at 100 µl per well and incubated at 37 °C for 30 min. The optical density was measured at 490 nm with a microplate reader (SpectraMAX ID3). For the colony

formation assay, cells were seeded into 6-well plates at a density of 2000 cells/well and cultured in medium composed of high-glucose DMEM with 10% FBS. The cells were allowed to grow for 2 weeks, and the medium was replaced every three days. After 14 days of cultivation, the cells were fixed with 4% polyoxymethylene and then stained with 0.1% crystal violet, imaged and counted. All experiments were repeated in triplicate, and each group had three duplicate wells.

Immunofluorescence

The cells were first seeded on chamber slides, followed by fixation using 4% paraformaldehyde and permeabilization with 0.1% Triton X-100. After that, the samples were blocked with 5% BSA at 25°C for 1 hour. The cells were then incubated overnight at 4°C with the primary antibody. After three PBS washes, the slides were incubated with the secondary antibody for 30 minutes at 25°C. Finally, the nuclei were stained with DAPI for easy visualization under a microscope.

Multicolor immunofluorescence(mIHC)

For Multicolor immunofluorescence(mIHC), cells were seeded on sterilized coverslips and cultured overnight to allow adherence. Cells were fixed with 4% paraformaldehyde at RT for 20 minutes, followed by permeabilization with 0.1% Triton X-100 in PBS on ice for 5 minutes. Blocking was carried out in PBS containing 2% bovine serum albumin (BSA) for 1 hour at RT. Primary antibodies against MOV10, CD163, and CD206 were incubated at 4°C overnight. The cells were then incubated with fluorescence-conjugated secondary antibodies at RT for 1 hour. Multiplexed fluorescence staining was performed using the multiplex immunohistochemical staining kit (abs50013, Absin, Shanghai, China). Finally, nuclei were stained with DAPI, and coverslips were mounted using an anti-fade mounting medium. Fluorescence images were acquired using a confocal microscope. All primary antibodies (MOV10,

CD163, and CD206) were purchased from RiboBio (Guangzhou, China).

Screening of autophagy-related differentially expressed genes and analysis of correlation with MOV10 expression

To explore the relationship between MOV10 and autophagy, we obtained a list of all autophagy-related genes from Human Autophagy Database （HADb）, screened differentially expressed autophagy genes from TCGA glioma expression matrix data, and then analysed the association between MOV10 and autophagy-related genes by Pearson's test.

Autophagic flux measurement

After initial treatment with siRNA for 48 h, the cells were digested and then reseeded in laser confocal dishes at a concentration of 5×10^4 cells/well. Next, OSTER Biological Technology, Wuhan, China) and placed in the dark until detection. Autophagic flux was quantified using a STELLARIS 5 Laser confocal microscope (Leica, Germany). Yellow dots indicated autophagosomes, and red dots represented autolysosomes.

Flow cytometry assay

The proportion of apoptotic cells was quantified by an Annexin V-FITC apoptosis detection kit (Beyotime, Shanghai, China). After 48 h of transfection, the cell supernatant was collected, and the cells were digested with EDTA-free trypsin and then centrifuged together to remove the supernatant. Next, the cell precipitate was washed in PBS and subjected to another round of centrifugation, and the supernatant was discarded again. Then, the cells were resuspended in Annexin V-FITC Binding Buffer. Immediately before flow cytometry, the cells were treated with Annexin V-FITC and PI dye solution according to the manufacturer's instructions. Finally, the cells were incubated at ambient temperature without light exposure for 10-15 min and detected by FC 500 flow cytometry (Beckman

Coulter, Bethesda, Massachusetts, United States).

Statistical analysis

Differences between the groups were analyzed using the log-rank test, and the "ggplot2" package was used for data visualization. To compare differences between groups, unpaired t-tests were applied. Univariate and multivariate Cox regression analyses were performed to create a Cox proportional hazards model. Pearson's non-parametric test was used for correlation analysis, while survival analysis was carried out using the "survminer" package in R. A threshold of $P < 0.05$ was set for statistical significance. All statistical analyses were conducted using R (version 4.3.1) and Perl (version 5.32.1.1).

Results

Upregulated expression of MOV10 in glioma is associated with poor prognosis of glioma patients

Overexpression of MOV10 in glioma is associated with poor patient prognosis. By examining the mRNA expression of MOV10 in various cancers using the GEPIA2 database, we found that MOV10 was significantly upregulated in a variety of cancers (relative to normal tissues) ((Figure 1A), especially in GBM. This result was further supported by the analysis of the TCGA database ($p < 0.05$) (Figure 1B). Kaplan-Meier survival analysis showed that patients with high MOV10 expression had a significantly worse survival rate than those with low expression (Figure 1C-D). To investigate the correlation between MOV10 expression and clinical characteristics, we downloaded the expression data and clinical information of 693 glioma patients from the CGGA database. Our analysis showed that there were significant differences in the expression of MOV10 in different clinical subgroups, and that the expression of MOV10 was closely associated with tumor recurrence, malignancy, IDH mutation status, and 1p/19q co-deletion

status (Figure 1E-H). Therefore, MOV10 may be an important molecular marker for evaluating the biological behavior and prognosis of glioma.

Generation of a prognostic model incorporating MOV10 expression in glioma based on CGGA and TCGA data.

To further study how MOV10 affects patient prognosis, we used the CGGA database, retained valid sample data, and grouped patients according to clinical characteristics. The groups included disease grade (III, IV, and II), age group (Age) (<40 years and ≥40 years), gender group (Gender) (male and female), IDH mutation status (IDH.mutation.status) (wild type and mutant), and 1p/19q co-deletion status (codel and non-codel). Cox regression analysis showed that MOV10 expression ($p < 0.001$, HR=1.680, 95%CI: 1.350-2.090), tumor grade ($p < 0.001$, HR=4.370, 95%CI: 3.140-6.080), PRS type (Primary Recurrent or Secondary) ($p < 0.001$, HR=2.160, 95%CI: 1.730-2.680), IDH mutation status ($p < 0.001$, HR=3.060, 95%CI: 2.460-3.820), 1p/19q co-deletion status ($p < 0.001$, HR=3.706, 95%CI: 2.550-5.020), and age ($p < 0.001$, HR=1.630, 95%CI: 2. 95%CI: 2.95%CI: 1.300-2.040) is an important risk factor for glioma prognosis. In addition, Cox multivariate analysis of tumor patient samples from CGGA and TCGA-GBM revealed that MOV10 could also serve as an independent risk factor for patient prognosis (Figure 2A, Figure S1A). Using the CGGA and TCGA databases, we generated ROC curves for 1-, 3-, and 5-year overall survival rates, with AUC values of 0.71, 0.76, 0.74, 0.718, 0.747, and 0.738, respectively, all higher than 0.6, suggesting that MOV10 expression is a reliable predictor of patient survival (Figure 2B, Figure S1B). The nomogram and calibration plot further validated the predictive accuracy of the model. The nomogram showed that the higher the score, the worse the prognosis, and the calibration plot showed that the predicted survival curve had good consistency with the ideal survival curve (Figure 2C, Figure S1C-E). In addition, survival curve analysis showed that higher tumor grade, and recurrence were associated with poor survival outcomes (Figure

2D-G).

Co-Expression Analysis and Enriched Pathways Associated with MOV10

To further investigate the functional role of MOV10 in glioma, we extracted the top 1000 genes co-expressed by MOV10 from the cBioPortal database and performed GO and KEGG enrichment analysis. GO enrichment analysis showed that these genes were mainly associated with the regulation of RNA splicing and mRNA metabolic processes (Figure 3A), while KEGG analysis highlighted their involvement in nuclear transport, mRNA surveillance pathways, and ATP-dependent chromatin remodeling[55] (Figure 3B). We integrated glioma expression data using the TCGA-R software package and analyzed the expression profile of MOV10. The samples were divided into high-expression and low-expression groups according to the median expression level of MOV10 mRNA, and differential expression analysis identified 1599 upregulated DEGs and 1051 downregulated DEGs (Figure 3C). GSEA enrichment analysis showed that the high-expression MOV10 group was enriched in pathways such as interferon-γ response, allograft rejection, and epithelial-mesenchymal transition compared with the low-expression group (Figure 3D-E). These results provide important insights for further exploring the role of MOV10 in glioma and other related diseases.

MOV10 is highly expressed in glioma tissues and cell lines

Based on the bioinformatics analysis of TCGA and CGGA databases, it was found that compared with that in normal brain tissues from trauma patients, MOV10 expression was significantly higher in glioma tissues. To further verify the bioinformatics analysis results, 81 glioma tissues and 29 normal brain injury tissues were collected in Jiangxi Cancer Hospital. The expression level of MOV10 was verified by RT-qPCR. MOV10 was significantly increased in glioma tissues (Figure. 4A), and the results were consistent with bioinformatics analysis. Similarly, three glioma cell lines

(U87 U251 T98G) exhibited significantly higher MOV10 expression than human astroglial normal cells (HEB) (Figure. 4B). T98G and U251 cell lines were used in the follow-up experiment.

MOV10 Knockdown Inhibits Proliferation, Migration, and Invasion of Glioma Cells

To study the biological function of MOV10 in glioblastoma (GBM), we performed gene silencing experiments using two siRNAs targeting MOV10. RT-qPCR (Figure 4C-D) and Western blotting (WB) (Figure 4E-F) confirmed efficient MOV10 knockdown in U251 and T98G cells. EDU and MTS assays showed that siMOV10 slowed the proliferation rate of glioma cells (Figure 4G-H，Figure S2A-B), and clonogenic assays revealed fewer colony-forming cells in the MOV10 knockdown group (Figure 4I). Additionally, the expression of proliferation-related proteins CDK6 and cyclin D1 was significantly decreased (Figure 4C), indicating that MOV10 knockdown inhibits glioma cell proliferation. Furthermore, transwell and wound-healing assays demonstrated that MOV10 knockdown significantly reduced the migration and invasion abilities of U251 and T98G cells (Figures 5A-B). Western blot analysis of EMT-related proteins, including N-cadherin and MMP2, revealed significantly decreased expression compared with the NC group (Figure 5C). These findings suggest that MOV10 promotes glioma cell migration and invasion through EMT-related phenotypic changes.

MOV10 expression is associated with TME characteristics, immune checkpoint expression, immune cell infiltration, and immunotherapy response

To investigate the connection between MOV10 and the tumor immune microenvironment, we performed ESTIMATE analysis on the integrated TCGA-glioma dataset. According to the expression of MOV10, the median was divided into high and low groups. The findings showed that glioma samples

with high MOV10 expression had significantly higher stromal, ESTIMATE, and immune scores compared to the low-expression group, suggesting that MOV10 overexpression is linked to a more complex tumor microenvironment and greater immune cell infiltration (Fig. 6A). Correlation and Kaplan-Meier (KM) analysis demonstrated that high MOV10 expression was positively correlated with higher ESTIMATE, immune, and stromal scores, and patients with higher scores had poorer prognoses (Fig. 6B-C). This indicates that MOV10 may play a critical role in modulating the glioma microenvironment. To verify these results, we applied the xCell algorithm, which revealed consistent differences in immune, stromal, and microenvironment scores between the high and low MOV10 expression groups (Fig. 6D-E), and showed that high MOV10 expression was associated with higher levels of macrophages and epithelial cells. These discoveries offer significant insights into MOV10's function and its potential as a therapeutic target. CiberSort immune infiltration analysis identified differences in macrophages, NK cells resting, and monocytes related to MOV10 expression, with a positive correlation with macrophages and a negative correlation with memory B cells and naive CD4+ T cells (Fig. 6F-G). TIDE analysis showed significantly higher TIDE scores in the MOV10 high-expression group, indicating a stronger immune-evasion signature and suggesting that MOV10 may contribute to tumor immune escape (Fig. S3F). Moreover, ssGSEA/GSVA-based exhaustion subtype analysis revealed that, within the MOV10-high group, the Terminal_Tex score was significantly higher than the Progenitor_Tex score (paired comparison, P = 4.5e-07; Fig. S4A). This pattern suggests that MOV10-high tumors are dominated by a deep/terminal, largely non-reinvigoratable exhaustion state rather than a progenitor-like reversible phenotype, consistent with the elevated TIDE-predicted poor response to anti-PD-1/anti-CTLA-4 therapy..Additionally, correlation and differential analysis showed that most immune checkpoints and immune-related genes were significantly associated with high MOV10 expression (Fig. 6H-I).

To further investigate the relationship between immunity and MOV10, we integrated WGCNA and CIBERSORT analyses. By combining MOV10-upregulated differentially expressed genes (DEGs) in TCGA samples with the MOV10-CIBERSORT results, we found that the expression of MOV10-upregulated DEGs was predominantly enriched in M0 macrophages and M2 macrophages (Fig. S3A). This suggests a potential functional association between MOV10 and these immune cell subtypes.To refine the module identification, we set the soft-thresholding power to 0.85, resulting in more accurate enrichment of relevant modules (Fig. S3B). Using a gene clustering dendrogram (Cluster Dendrogram) coupled with dynamic tree cutting (Dynamic Tree Cut) and merged dynamic modules, we identified two gene modules: the brown module (MEbrown) and turquoise module (MEturquoise) (Fig. S3C).Correlation analysis revealed that these two modules were highly associated with M0 macrophages and M2 macrophages, with the turquoise module (enriched with MOV10-related genes) showing a significant positive correlation with M2 macrophages (Fig. S3D-E). This highlights a potential role of MOV10 in regulating M2 macrophage-related functions.

Silencing MOV10 inhibits the invasion of M2 macrophages in glioma

To further investigate the biological significance of MOV10 and macrophages, we performed cell experiments and immunofluorescence analysis. We first established the M2 model of macrophage THP-1 (Figure 7A-B). To confirm that THP-1 cells were successfully polarized into M2 macrophages, we used M2 markers CD163 and CD206 and analyzed protein expression in M0 and M2 macrophages by Western blotting. The results showed that the expression of these proteins was significantly increased in M2 cells. Immunofluorescence analysis showed that CD163 and CD206 were mainly localized in M2 macrophages (Figure 7C-E). Multicolor immunofluorescence analysis showed that MOV10 co-localized with CD206 and CD163 in human glioma tissue, indicating that MOV10 is associated with

M2 macrophages and may affect their functional properties in the tumor microenvironment (Figure 7F, Figure S4B-C). In addition, To clarify the glioma–macrophage interaction, we performed a transwell co-culture assay in which THP-1–derived M2 macrophages were seeded in the upper chamber and glioma cells (T98G or U251) transfected with siMOV10 were placed in the lower chamber. MOV10 silencing in glioma cells significantly reduced the number of invading M2 macrophages compared with controls, indicating that glioma-cell–derived MOV10 promotes M2 macrophage invasiveness via paracrine signaling. (Figure 7G-H).

MOV10 knockdown enhances autophagy and apoptosis in glioma cells

To investigate the role of MOV10 in glioma, we first analyzed the correlation between MOV10 and autophagy. Among the 1599 upregulated genes obtained from TCGA glioma data, 16 were related to autophagy (Fig. 8A). Pearson correlation analysis further revealed that several differentially expressed genes associated with autophagy, including CASP1, CASP4, CASP8, ITGB4, NAMPT, and SERPINA1, were positively correlated with MOV10 expression (Fig. 8B). To further explore whether MOV10 affects glioma cell development through autophagy, we used the mRFP-GFP reporter adenovirus labeled with LC3 to assess autophagic flux. The results showed an increase in yellow and red spots after silencing MOV10 (Fig. 9A), indicating enhanced autophagy. Additionally, the downregulation of p62 protein and the increased LC3II/LC3I ratio also indicated increased autophagy levels (Fig. 9C), suggesting that MOV10 can regulate autophagy in U251 and T98G cells.Further investigation into the mechanism of MOV10 in glioma revealed that 48 hours after transfection of siMOV10, apoptosis levels were significantly higher in the siMOV10 group compared to the NC group, as determined by Annexin V-FITC flow cytometry (Fig. 9B). Western blot assays also showed increased expression of Bax and decreased expression of Bcl-2 (Fig. 9C), indicating that MOV10 knockdown promotes

apoptosis in U251 and T98G cells.

Discussion

Gene therapy, which involves introducing or modifying genes in target cells, is widely used in cancer treatment [20]. In this study, we used TCGA data to assess MOV10 expression across 33 tumor types and found that MOV10 is overexpressed in gliomas and is linked to poor prognosis. Validation using glioma samples and normal brain samples confirmed that MOV10 could potentially serve as a diagnostic marker for gliomas. Studies have shown that MOV10 downregulates the tumor suppressor INK4a through interaction with the PRC1 complex [22]. Additionally, MOV10 has been found to interact with breast cancer anti-estrogen resistance protein 1 in lung adenocarcinoma, suggesting a possible role in tumor progression [23-24]. Further analysis of TCGA and CGGA data reinforced that high MOV10 expression is associated with worse outcomes, higher cancer grade, older age, and PRS type in gliomas. Univariate Cox regression analysis identified MOV10 as a risk factor for gliomas. The nomogram we developed, which integrates MOV10 expression and clinical data, accurately predicted 1-year, 3-year, and 5-year overall survival (OS), providing valuable insights for patient stratification and treatment planning.

Uncontrolled cell proliferation is a hallmark of malignant tumor development and progression, often driven by aberrant proliferation signals [25, 26]. Functional enrichment analysis revealed that MOV10 is primarily involved in pathways such as interferon-γ response, allograft rejection, and EMT. Interferon-γ response contributes to antiviral defense, macrophage activation, and enhanced antigen presentation. GO and KEGG analyses also showed that MOV10 is enriched in pathways regulating mRNA metabolism and RNA splicing. Clonogenic and MTS analyses showed that knockout of MOV10 significantly reduced cell colony formation and proliferation, while downregulating the expression of CDK6 and CyclinD1, indicating that MOV10

regulates cell proliferation by affecting the cell cycle. EMT-like processes are crucial in tumorigenesis, invasion, metastasis, and drug resistance [27, 28]. Although true EMT involves a transition from an epithelial to a mesenchymal state, a similar process can be observed in gliomas, where cells exhibit EMT-like characteristics, such as enhanced migration and invasion. Overexpression of MOV10 has been shown to promote the proliferation and invasion of pancreatic cancer cells but inhibit the invasion and migration of melanoma cells [11,29]. Our studies further support this notion, as transwell and wound wound assays confirmed that MOV10 knockdown significantly inhibited the invasion and migration of T98G and U251 cells, and reduced the expression of MMP2 and N-cadherin. These findings suggest that MOV10 drives the malignant behavior of gliomas by promoting EMT-like processes (characterized by increased cell proliferation and invasion), rather than true EMT. The role of MOV10 in regulating these processes highlights its potential as a key regulator of glioma progression.

Immunotherapy holds great promise in cancer treatment. We examined the correlation between MOV10 expression and immune cell infiltration in tumors. CD8+ T cells are key drivers of anti-tumor immunity, and low infiltration of these cells is linked to immune suppression and poorer survival outcomes [30, 31]. Our analysis revealed that MOV10 is negatively associated with CD8+ T cell infiltration in glioma, suggesting that MOV10 might contribute to immune evasion in gliomas. CD4+ T cells help regulate tumor immune responses [32], while M2 macrophages, through their interactions with tumor-inhibiting cells, have tumor-promoting and anti-inflammatory effects [33, 34]. Our results showed a positive correlation between high MOV10 expression and macrophage infiltration, particularly M2 macrophages, in glioma patients. Furthermore, MOV10 expression was positively associated with dendritic cells, NK cell resting, and CD4+ memory T cells. These findings indicate that MOV10 overexpression plays a crucial role in immune evasion in gliomas, promoting tumor growth and progression.

Immune checkpoints play a key role in regulating immune activity, and their over- or underexpression can result in immune dysfunction [35]. T cell exhaustion is a major contributor to tumor-induced immune dysfunction [36]. In this study, MOV10 expression was positively associated with multiple T-cell exhaustion and immunosuppressive checkpoint markers, including PDCD1, CTLA4, HAVCR2, and CD274 (PD-L1), all of which are closely linked to responses to immune checkpoint blockade therapies [37]. The high expression of T cell exhaustion and immune checkpoint markers is associated with poor prognosis and may explain MOV10's tumor-promoting role. Tumor mutation burden (TMB) is a predictor of immunotherapy efficacy, reflecting the tumor's ability to generate neoantigens [38]. Furthermore, TIDE analysis showed a significantly higher TIDE score in the MOV10 high-expression group, indicating that this type of model is more likely to exhibit immune escape and therefore has a poorer predictive response to anti-PD-1/anti-CTLA-4 combined immunotherapy. This result is consistent with the immunosuppressive characteristics we observed[39, 40]. By studying macrophages in glioma cell lines, it was found that silencing MOV10 significantly inhibited the invasive ability of M2 macrophages, highlighting its role in immunosuppression. The accumulation of M2 macrophages and their proximity to blood vessels create an environment conducive to tumor growth and invasion [41]. MOV10 expression was significantly positively correlated with stromal and immune cell scores, and higher scores were associated with lower OS, suggesting that MOV10 may regulate tumor immunity through both stromal and immune cells in the TME. Further studies are needed to elucidate the exact mechanisms involved.

Autophagy plays a dual role in cancer development. On one side, it acts as a defense mechanism by degrading abnormal proteins and organelles to suppress cancer cell expansion [42]; on the other side, it can protect cancer cells, thereby promoting cancer progression [43, 44]. Deciding whether to enhance or inhibit autophagy in cancer treatment remains a critical question.

In our analysis of TCGA glioma data, we found that MOV10 is positively correlated with several autophagy-related molecules, including CASP1, CASP4, CASP8, ITGB4, NAMPT, and SERPINA1, which have been reported to regulate autophagy in cancer [45-50]. We hypothesized that MOV10 plays a role in autophagy regulation, and our in vitro experiments supported this. Knockdown of MOV10 increased the number of autophagosomes and autolysosomes, decreased p62 expression, and raised the LC3II/LC3I ratio, indicating heightened autophagy. Previous studies have shown that enhancing autophagy can suppress breast cancer metastasis and have anti-glioma effects [51-53]. These findings suggest that MOV10 knockdown may inhibit glioma cell survival by promoting autophagy.

Evasion of apoptosis is a key factor in tumor progression [54, 56], and inducing apoptosis is a major target in cancer treatment. In this study, knocking out MOV10 significantly enhanced apoptosis in U251 and T98G cells, a result further validated at the protein level. Previous research has similarly shown that MOV10 affects apoptosis sensitivity in pancreatic and lung adenocarcinoma cells [11, 23], aligning with our findings. MOV10's inhibition of apoptosis in glioma cells could be a novel therapeutic approach.

Although our results suggest that silencing MOV10 expression can inhibit tumor malignant proliferation and accelerate the cell cycle by promoting EMT, apoptosis, and autophagy, these findings require further in vivo validation and investigation of the underlying mechanisms. Bioinformatics analysis revealed that MOV10 is closely associated with immune cell infiltration in gliomas, and its high expression is associated with poor immunotherapy efficacy. Further investigation of MOV10 as a potential anti-glioma therapeutic target is warranted.

Conclusion

Based on analysis of the TCGA and CGGA databases and clinical tissue samples, we proved for the first time that MOV10 is highly expressed in

gliomas and is highly correlated with immune cell infiltration.Immunological experiments such as mIHC confirmed that MOV10 is expressed in M2 macrophages. In addition, MOV10 knockdown inhibits cell proliferation, invasion and migration, regulates autophagy and promotes apoptosis. In short, MOV10 is an important molecule in the regulation of gliomas, and our findings provide a promising target for the treatment of gliomas.

Appendix

Acknowledgements

Not applicable.

Funding

This work was supported by the National Natural Science Foundation of China (No.82060680, 82360736), The Distinguished Young Scholars program of the Natural Science Foundation of Jiangxi Province (20224ACB216015), Science and Technology Plan of Health Commission of Jiangxi Provincial (202310059), Science and Technology Research Project of Jiangxi Provincial Department of Education (GJJ2203508), Open Research Fund of Jiangxi Cancer Hospital & Institute (KFJJ2023ZD05), The"Five-level Progressive" talent cultivation project of Jiangxi Cancer Hospital & Institute (WCDJ2024YQ03).

Availability of data and materials

Not applicable.

Ethics approval and consent to participate

This study was approved by the Ethics Committee of Jiangxi Cancer Hospital (2020ky008)

Competing interests

The authors declare that they have no conflicts of interest.

Consent for publication

Not applicable.

Data availability

The datasets generated and/or analyzed during the current study are

available in the [CGGA] repository [https://www.cgga.org.cn]; the [UCSC] repository [https://xenabrowser.net/datapages]; the [cbioportal] repository [https://www.cbioportal.org]; and the [TIDE] repository [http://tide.dfci.harvard.edu]. These datasets are all public datasets. Other datasets used in the current study are noted in the Methods section. We will provide some code for your publication if you require code reproduction.The datasets used and/or analysed during the current study available from the corresponding author on reasonable request.

Authors' contributions

Shuhui Chen: Project administration, Methodology, Formal analysis, Conceptualization. Linlin Ruan: Methodology, Formal analysis, Conceptualization. Feiyu Wang: Writing – original draft. Wenbin Yang: Methodology. Yueben Hu: Writing – review & editing. Yangzhon Guo: Methodology. Xuanxuan Xiong: Methodology. Dan Liu: Writing – review & editing, Validation. Qiaoli Lv: Writing – review & editing, Validation, Conceptualization.

Author details

Feiyu Wang, School of Chemistry and Bioengineering, Yichun College, Yichun 336000, Jiangxi, China. Email address: wfy18012069088@163.com

Linlin Ruan, Jiangxi Key Laboratory of oncology(2024SSY06041), JXHC Key Laboratory of Tumour Metastasis, Jiangxi Cancer Hospital & Institute, The Second Affiliated Hospital of Nanchang Medical College, Nanchang, 330006, China. E-mail address: RLL10351259771128@163.com

Wenbin Yang, School of pharmacy, Nanchang University, Nanchang, 330006, China. E-mail address: Y1112cute@163.com

Yueben Hu, Department of Pharmacy, Nanchang People's hospital(Nanchang Third hospital), Nanchang, 330009, P.R. China, E-mail address: hybstrive@163.com

Yangzhon Guo, Jiangxi Key Laboratory of oncology(2024SSY06041), JXHC Key Laboratory of Tumour Metastasis, Jiangxi Cancer Hospital & Institute,

The Second Affiliated Hospital of Nanchang Medical College, Nanchang, 330029, P.R. China, E-mail address: yangzg23@foxmail.com

Xuanxuan Xiong, Jiangxi Provincial Key Laboratory of Basic Pharmacology, Nanchang University School of Pharmaceutical Science, Nanchang, 330006, China. E-mail address: xuanxuanxiong@163.com

Dan Liu, Jiangxi Provincial Key Laboratory of Basic Pharmacology, Nanchang University School of Pharmaceutical Science, Nanchang, 330006, China. E-mail address: ld1201jx@ncu.edu.cn

*Corresponding authors:

Shuhui Chen, Jiangxi Key Laboratory of oncology(2024SSY06041), JXHC Key Laboratory of Tumour Metastasis, Jiangxi Cancer Hospital & Institute, The Second Affiliated Hospital of Nanchang Medical College, Nanchang, 330029, China. E-mail address: chenshuhui2008@126.com

Qiaoli Lv, Jiangxi Key Laboratory of oncology(2024SSY06041), JXHC Key Laboratory of Tumour Metastasis, Jiangxi Cancer Hospital & Institute, The Second Affiliated Hospital of Nanchang Medical College, Nanchang, 330029, China. E-mail address: lvqiaoli2008@163.com

Reference

[1] Aldape K, Brindle K M, Chesler L, et al. Challenges to curing primary brain tumours[J]. *Nat Rev Clin Oncol*, 2019, 16(8): 509-520.

[2] Zhang L, Min Z, Tang M, et al. The utility of diffusion MRI with quantitative ADC measurements for differentiating high-grade from low-grade cerebral gliomas: Evidence from a meta-analysis[J]. *J Neurol Sci*, 2017, 373: 9-15.

[3] Chen R, Smith-Cohn M, Cohen A L, et al. Glioma Subclassifications and Their Clinical Significance[J]. *Neurotherapeutics*, 2017, 14(2): 284-297.

[4] Ostrom QT, Price M, Neff C, et al. CBTRUS Statistical Report: Primary Brain and Other Central Nervous System Tumors Diagnosed in the United States in 2016-2020. Neuro Oncol. 2023;25(12 Suppl 2):iv1-iv99.

[5] Chen J, Li Y, Yu T S, et al. A restricted cell population propagates glioblastoma growth after chemotherapy[J]. *Nature*, 2012, 488(7412): 522-526.

[6] Gregersen L H, Schueler M, Munschauer M, et al. MOV10 Is a 5' to 3' RNA helicase contributing to UPF1 mRNA target degradation by translocation along 3' UTRs[J]. *Mol Cell*, 2014, 54(4): 573-585.

[7] Li S, Wang L, Berman M, et al. Mapping a dynamic innate immunity protein interaction network regulating type I interferon production[J]. *Immunity*, 2011, 35(3): 426-440.

[8] Nawaz A, Shilikbay T, Skariah G, et al. Unwinding the roles of RNA helicase MOV10[J]. *Wiley Interdiscip Rev RNA*, 2022, 13(2): e1682.

[9] Fairman-Williams M E, Guenther U P, Jankowsky E. SF1 and SF2 helicases: family matters[J]. *Curr Opin Struct Biol*, 2010, 20(3): 313-324.

[10] Nakano M, Kakiuchi Y, Shimada Y, et al. MOV10 as a novel telomerase-associated protein[J]. *Biochem Biophys Res Commun*, 2009, 388(2): 328-332.

[11] Yang D, Hu Z, Xu J, et al. MiR-760 enhances sensitivity of pancreatic cancer cells to gemcitabine through modulating Integrin beta1[J]. *Biosci Rep*, 2019, 39(11).

[12] He Q, Zhao L, Liu X, et al. MOV10 binding circ-DICER1 regulates the angiogenesis of glioma via miR-103a-3p/miR-382-5p mediated ZIC4 expression change[J]. J Exp Clin Cancer Res, 2019, 38(1): 9.

[13] Gangoso E, Southgate B, Bradley L, et al. Glioblastomas acquire

myeloid-affiliated transcriptional programs via epigenetic immunoediting to elicit immune evasion[J]. *Cell*, 2021, 184(9): 2454-2470.

[14] Zhang Y, Zhang Z. The history and advances in cancer immunotherapy: understanding the characteristics of tumor-infiltrating immune cells and their therapeutic implications[J]. *Cell Mol Immunol*, 2020, 17(8): 807-821.

[15] Morales E, Olson M, Iglesias F, et al. Role of immunotherapy in Ewing sarcoma[J]. *J Immunother Cancer*, 2020, 8(2).

[16] Alban T J, Bayik D, Otvos B, et al. Glioblastoma Myeloid-Derived Suppressor Cell Subsets Express Differential Macrophage Migration Inhibitory Factor Receptor Profiles That Can Be Targeted to Reduce Immune Suppression[J]. *Front Immunol*, 2020, 11: 1191.

[17] Goodier J L, Cheung L E, Kazazian H J. MOV10 RNA helicase is a potent inhibitor of retrotransposition in cells[J]. *PLoS Genet*, 2012, 8(10): e1002941.

[18] Song Z W, Ma Y X, Fu B Q, et al. Altered mRNA levels of MOV10, A3G, and IFN-alpha in patients with chronic hepatitis B[J]. *J Microbiol*, 2014, 52(6): 510-514.

[19] Jung H, Choi J K, Lee E A. Immune signatures correlate with L1 retrotransposition in gastrointestinal cancers[J]. *Genome Res*, 2018, 28(8): 1136-1146.

[20] Gruntman A M, Flotte T R. The rapidly evolving state of gene therapy[J]. *FASEB J*, 2018, 32(4): 1733-1740.

[21] Xin Y, Huang M, Guo W W, et al. Nano-based delivery of RNAi in cancer therapy[J]. *Mol Cancer*, 2017, 16(1): 134.

[22] El M S, Nicholls J, Maertens G N, et al. Role for the MOV10 RNA helicase in polycomb-mediated repression of the INK4a tumor

suppressor[J]. *Nat Struct Mol Biol*, 2010, 17(7): 862-868.

[23] Mao C G, Jiang S S, Shen C, et al. BCAR1 promotes proliferation and cell growth in lung adenocarcinoma via upregulation of POLR2A[J]. *Thorac Cancer*, 2020, 11(11): 3326-3336.

[24] Turkalp Z, Karamchandani J, Das S. IDH mutation in glioma: new insights and promises for the future[J]. *JAMA Neurol*, 2014, 71(10): 1319-1325.

[25] Gao F, Xu T, Wang X, et al. CIP2A mediates fibronectin-induced bladder cancer cell proliferation by stabilizing beta-catenin[J]. *J Exp Clin Cancer Res*, 2017, 36(1): 70.

[26] Ingham M, Schwartz G K. Cell-Cycle Therapeutics Come of Age[J]. *J Clin Oncol*, 2017, 35(25): 2949-2959.

[27] Pastushenko I, Blanpain C. EMT Transition States during Tumor Progression and Metastasis[J]. *Trends Cell Biol*, 2019, 29(3): 212-226.

[28] Cho E S, Kang H E, Kim N H, et al. Therapeutic implications of cancer epithelial-mesenchymal transition (EMT)[J]. *Arch Pharm Res*, 2019, 42(1): 14-24.

[29] Wang W, Snyder N, Worth A J, et al. Regulation of lipid synthesis by the RNA helicase Mov10 controls Wnt5a production[J]. *Oncogenesis*, 2015, 4: e154.

[30] Ostroumov D, Fekete-Drimusz N, Saborowski M, et al. CD4 and CD8 T lymphocyte interplay in controlling tumor growth[J]. *Cell Mol Life Sci*, 2018, 75(4): 689-713.

[31] Dolina J S, Van Braeckel-Budimir N, Thomas G D, et al. CD8(+) T Cell Exhaustion in Cancer[J]. *Front Immunol*, 2021, 12: 715234.

[32] Kim H J, Cantor H. CD4 T-cell subsets and tumor immunity: the helpful and the not-so-helpful[J]. *Cancer Immunol Res*, 2014, 2(2): 91-98.

[33] Sadri M, Heidari S, Faridzadeh A, et al. Potential applications of macrophages in cancer immunotherapy. *Biomed Pharmacother*. 2024;178:117161.

[34] Najafi M, Hashemi Goradel N, Farhood B, et al. Macrophage polarity in cancer: A review. *J Cell Biochem*. 2019;120(3):2756-2765.

[35] Li B, Chan H L, Chen P. Immune Checkpoint Inhibitors: Basics and Challenges[J]. *Curr Med Chem*, 2019, 26(17): 3009-3025.

[36] Kouidhi S, Ben A F, Benammar E A. Targeting Tumor Metabolism: A New Challenge to Improve Immunotherapy[J]. *Front Immunol*, 2018, 9: 353.

[37] Morad G, Helmink B A, Sharma P, et al. Hallmarks of response, resistance, and toxicity to immune checkpoint blockade[J]. *Cell*, 2021, 184(21): 5309-5337.

[38] Rizvi N A, Hellmann M D, Snyder A, et al. Cancer immunology. Mutational landscape determines sensitivity to PD-1 blockade in non-small cell lung cancer[J]. *Science*, 2015, 348(6230): 124-128.

[39] Hill B S, Sarnella A, D'Avino G, et al. Recruitment of stromal cells into tumour microenvironment promote the metastatic spread of breast cancer[J]. *Semin Cancer Biol*, 2020, 60: 202-213.

[40] Zhan H X, Zhou B, Cheng Y G, et al. Crosstalk between stromal cells and cancer cells in pancreatic cancer: New insights into stromal biology[J]. *Cancer Lett*, 2017, 392: 83-93.

[41] Clavreul A, Menei P. Mesenchymal Stromal-Like Cells in the Glioma Microenvironment: What Are These Cells?[J]. *Cancers (Basel)*, 2020, 12(9).

[42] Galluzzi L, Pietrocola F, Bravo-San P J, et al. Autophagy in malignant transformation and cancer progression[J]. *EMBO J*, 2015, 34(7): 856-880.

[43] Amaravadi R, Kimmelman A C, White E. Recent insights into the function of autophagy in cancer[J]. *Genes Dev*, 2016, 30(17): 1913-1930.

[44] Towers C G, Thorburn A. Therapeutic Targeting of Autophagy[J]. *EBioMedicine*, 2016, 14: 15-23.

[45] Wang D, Zhang J, Jiang W, et al. The role of NLRP3-CASP1 in inflammasome-mediated neuroinflammation and autophagy dysfunction in manganese-induced, hippocampal-dependent impairment of learning and memory ability[J]. *Autophagy*, 2017, 13(5): 914-927.

[46] Meng L, Tian Z, Long X, et al. Prognostic autophagy model based on CASP4 and BIRC5 expression in patients with renal cancer: independent datasets-based study[J]. *Am J Transl Res*, 2020, 12(11): 7475-7489.

[47] Allavena G, Cuomo F, Baumgartner G, et al. Suppressed translation as a mechanism of initiation of CASP8 (caspase 8)-dependent apoptosis in autophagy-deficient NSCLC cells under nutrient limitation[J]. *Autophagy*, 2018, 14(2): 252-268.

[48] Sung J S, Kang C W, Kang S, et al. ITGB4-mediated metabolic reprogramming of cancer-associated fibroblasts[J]. *Oncogene*, 2020, 39(3): 664-676.

[49] Kozako T, Aikawa A, Ohsugi T, et al. High expression of NAMPT in adult T-cell leukemia/lymphoma and anti-tumor activity of a NAMPT inhibitor[J]. *Eur J Pharmacol*, 2019, 865: 172738.

[50] Xu J, Dai S, Yuan Y, et al. A Prognostic Model for Colon Cancer Patients Based on Eight Signature Autophagy Genes[J]. *Front Cell Dev Biol*, 2020, 8: 602174.

[51] Marsh T, Debnath J. Autophagy suppresses breast cancer metastasis by degrading NBR1[J]. *Autophagy*, 2020, 16(6): 1164-1165.

[52] Meyer N, Henkel L, Linder B, et al. Autophagy activation, lipotoxicity and lysosomal membrane permeabilization synergize to promote pimozide- and loperamide-induced glioma cell death[J]. *Autophagy*, 2021, 17(11): 3424-3443.

[53] Huang T, Xu T, Wang Y, et al. Cannabidiol inhibits human glioma by induction of lethal mitophagy through activating TRPV4[J]. *Autophagy*, 2021, 17(11): 3592-3606.

[54] Pistritto G, Trisciuoglio D, Ceci C, et al. Apoptosis as anticancer mechanism: function and dysfunction of its modulators and targeted therapeutic strategies[J]. *Aging (Albany NY)*, 2016, 8(4): 603-619.

[55] Kanehisa, M., Sato, Y., Kawashima, M., Furumichi, M., and Tanabe, M.; KEGG as a reference resource for gene and protein annotation[J]. *Nucleic Acids Res.* 44, D457-D462 (2016).

[56] Zhang, Haonan et al. Optimized Dynamic Network Biomarker Deciphers a High-Resolution Heterogeneity Within Thyroid Cancer Molecular Subtypes[J]. *Med Research* (2025): n. pag.

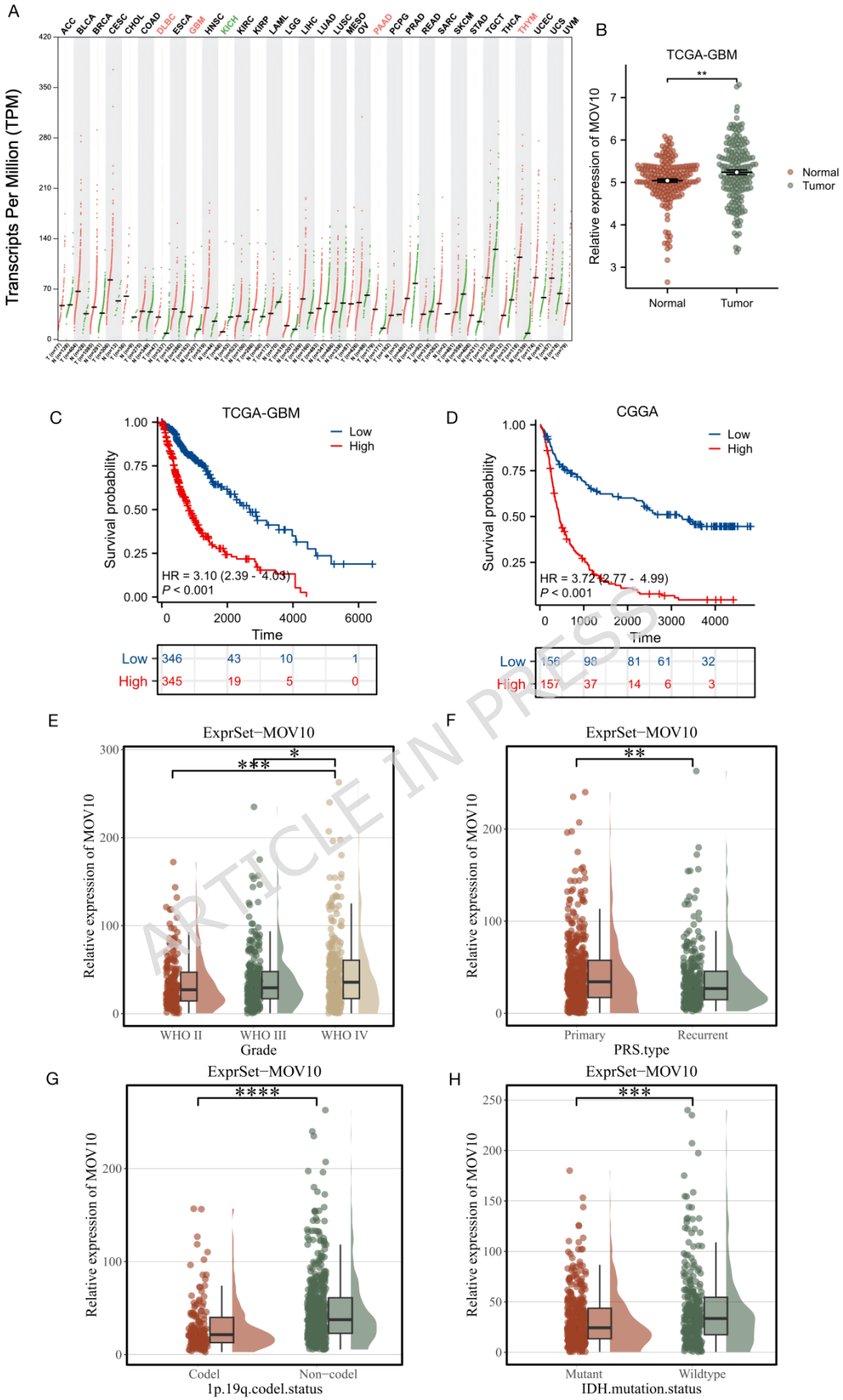

Figure 1: MOV10 is overexpressed in glioma and correlates with poor patient prognosis. A: GEPIA2 database shows the expression of MOV10 mRNA in

different cancer types. B: Differential expression of MOV10 in TCGA-GBM dataset. *p<0.05GBM vs normal. C-D: Overall survival curves of clinical feature groups in CGGA-TCGA glioma dataset. E-H: Expression and clinical differences of MOV10 in CGGA glioma dataset. *p<0.05. (***p<0.001, **p<0.01,*p<0.05).

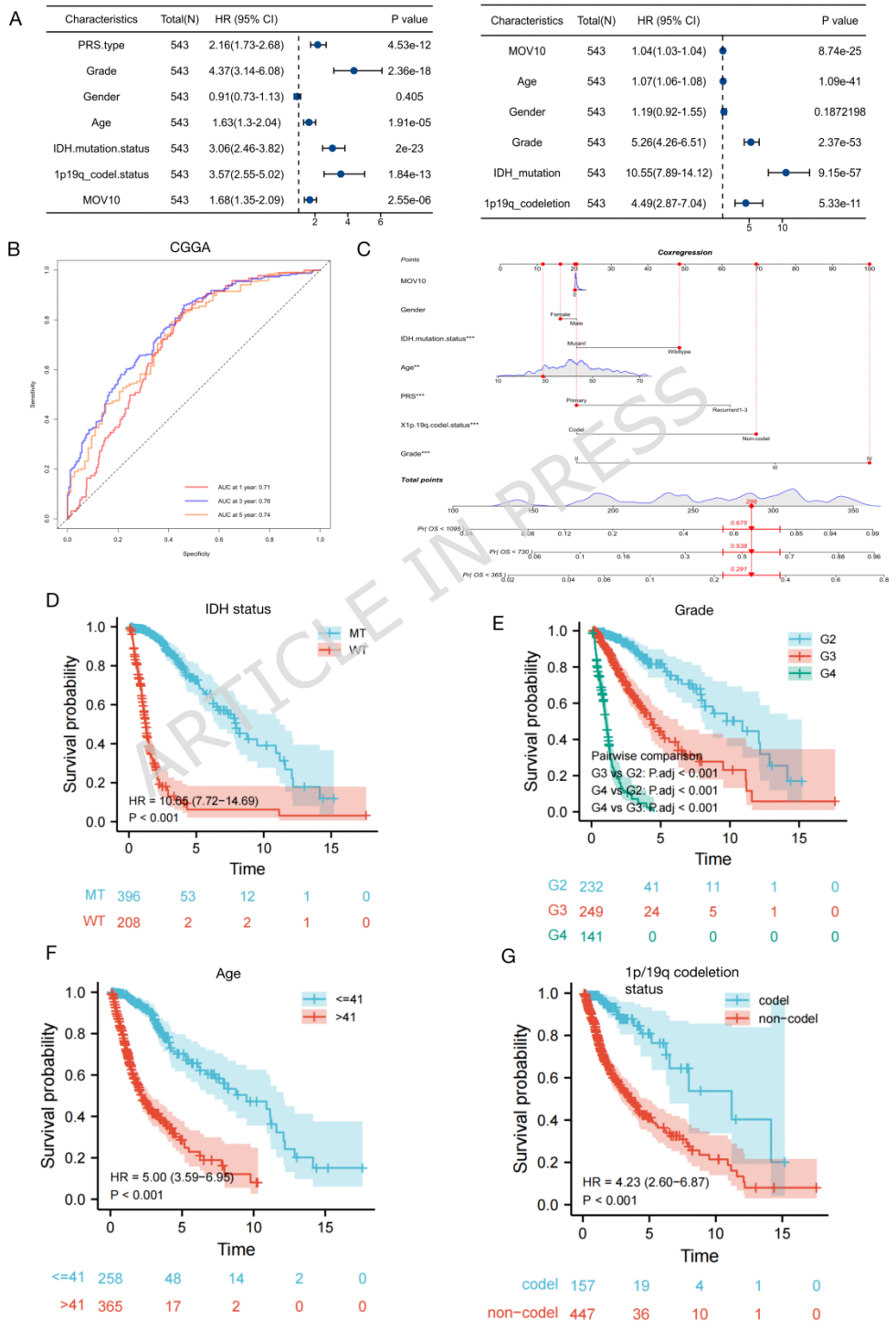

Figure 2: Creation of a prognostic model combining MOV10 expression in

glioma using CGGA and TCGA data. A: CGGA COX regression analysis evaluating the prognostic significance of MOV10 and other clinical factors in glioma. B: CGGA ROC curve showing the accuracy of the nomogram in predicting 1-, 3-, and 5-year OS. [AUC]: 0.71, 0.76, 0.74. C: Nomogram combining MOV10 expression with clinical characteristics of glioma patients based on CGGA data. The OS curves of clinical features group of glioma ,such as IDH status (D) ,grade (E), age(F), and 1p/19q codeletion status (G) .(***p<0.001, **p<0.01, *p<0.05).

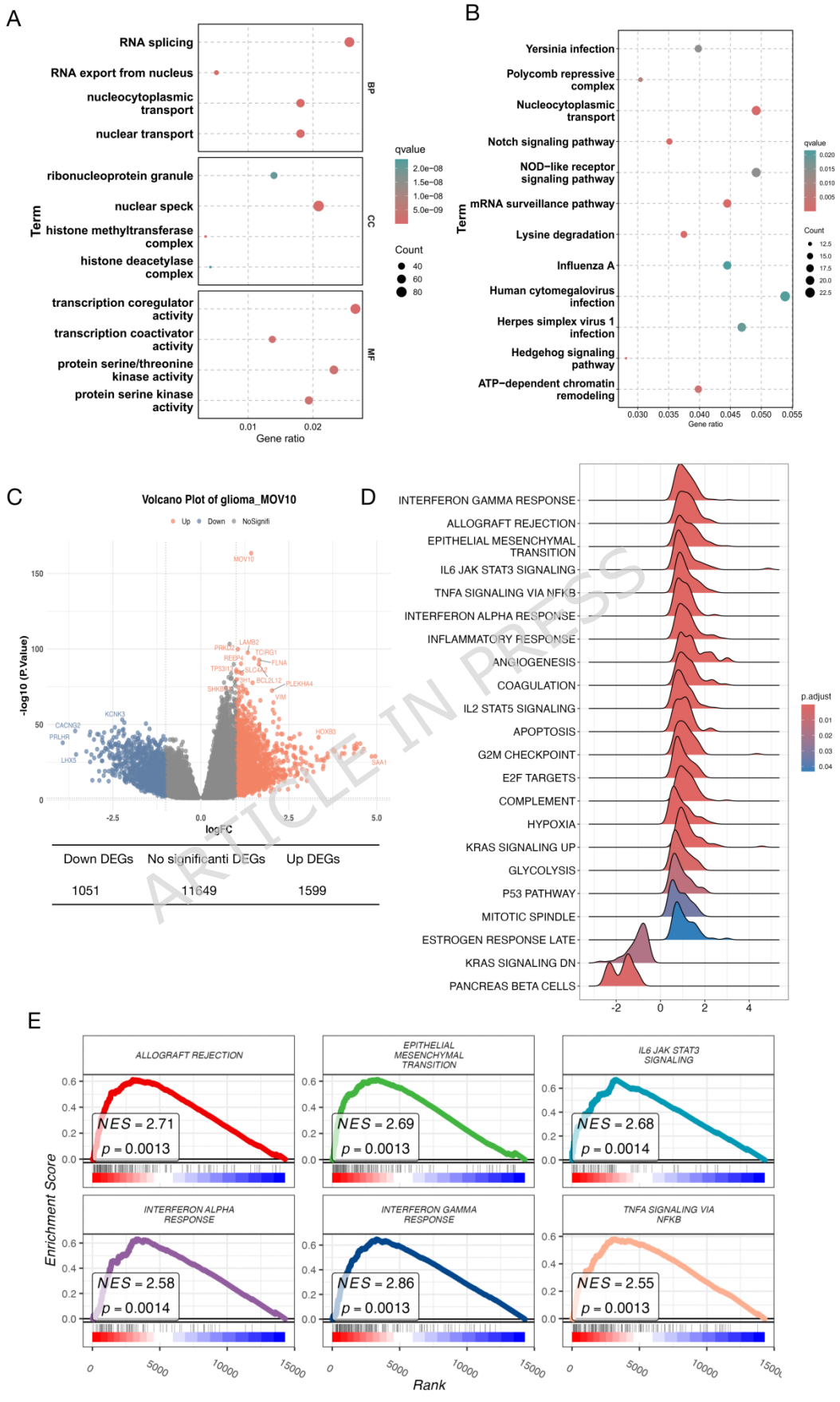

Figure 3: Functional enrichment of MOV10-associated genes in glioma. A:

Gene Ontology (GO) analysis of the top 1,000 MOV10 co-expressed genes in glioma. B: Kyoto Encyclopedia of Genes and Genomes (KEGG) analysis of the top 1,000 MOV10 co-expressed genes in glioma. C: Volcano plot depicting the differentially expressed genes (DEGs) related to MOV10. $p<0.05$ and $|log2FC| > 1.0$. high vs low. D: Gene set enrichment analysis (GSEA) ridge plot comparing high and low MOV10 expression groups in the TCGA-Glioma database. E: GSEA showing six enriched pathways in the high MOV10 expression group vs. the low MOV10 expression group in the TCGA-Glioma data base; criteria: NES>1, FDR<0.25.

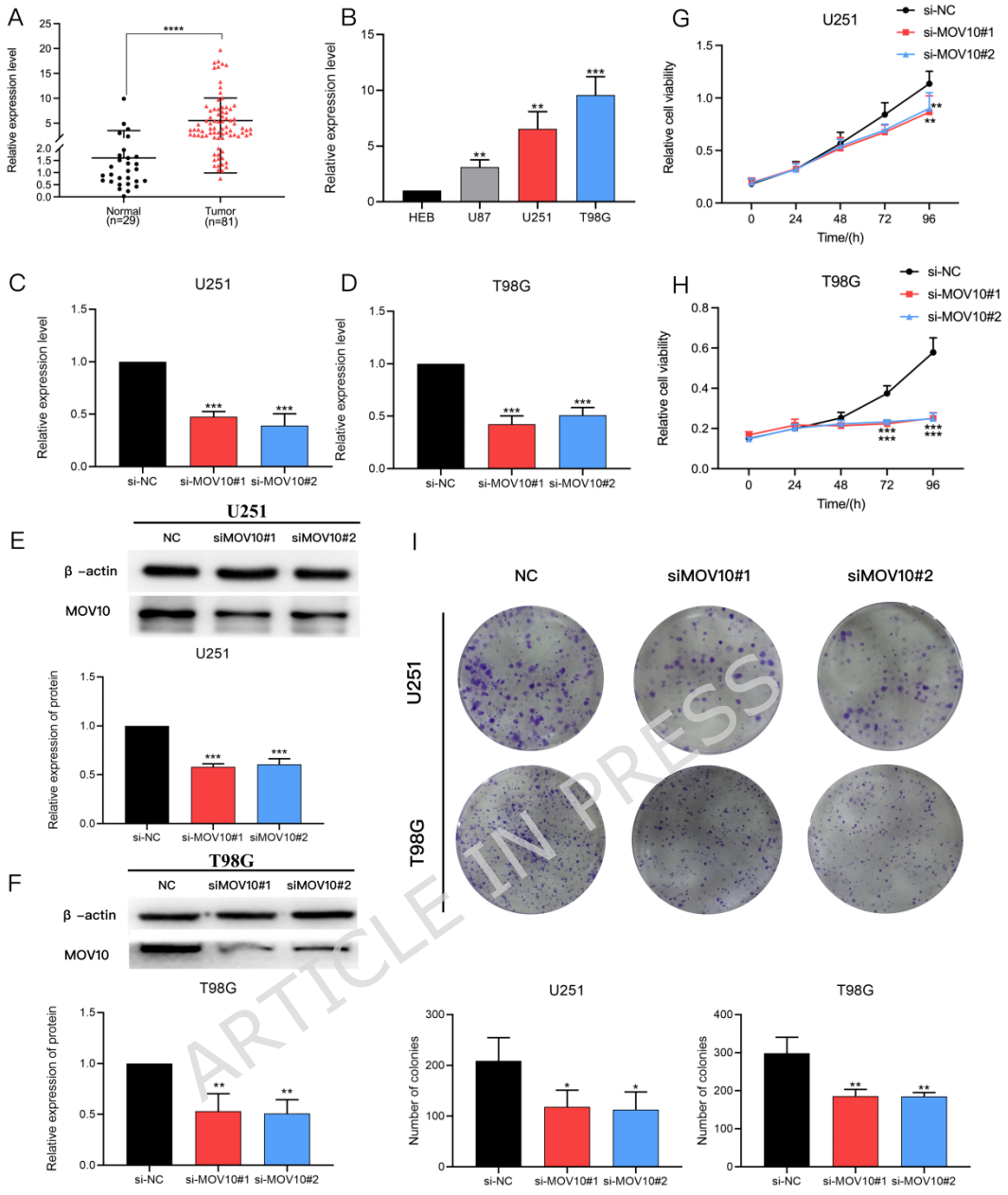

Figure 4: MOV10 was upregulated in glioma tissues and cell lines, and siMOV10 inhibited the proliferation of glioma cells. A: Comparison of MOV10 expression levels between 81 GBM tissues and 29 normal brain tissues by RT–qPCR. B: RT–qPCR analysis of the relative expression of MOV10 in the U87, U251, T98G and HEB cell lines. C-D: The expression level of MOV10 in T98G and U251 cells treated with two independent siRNAs was examined by RT–qPCR. E-F: The protein expression level of MOV10 in T98G and U251 cells treated with siMOV10. G-H: Knockdown by siMOV10 transfection

suppressed the proliferation of T98G and U251 cells, as shown by MTS assay. I: Knockdown of MOV10 impaired the clone formation ability of glioma cells (***p<0.001, **p<0.01, *p<0.05，n=3).

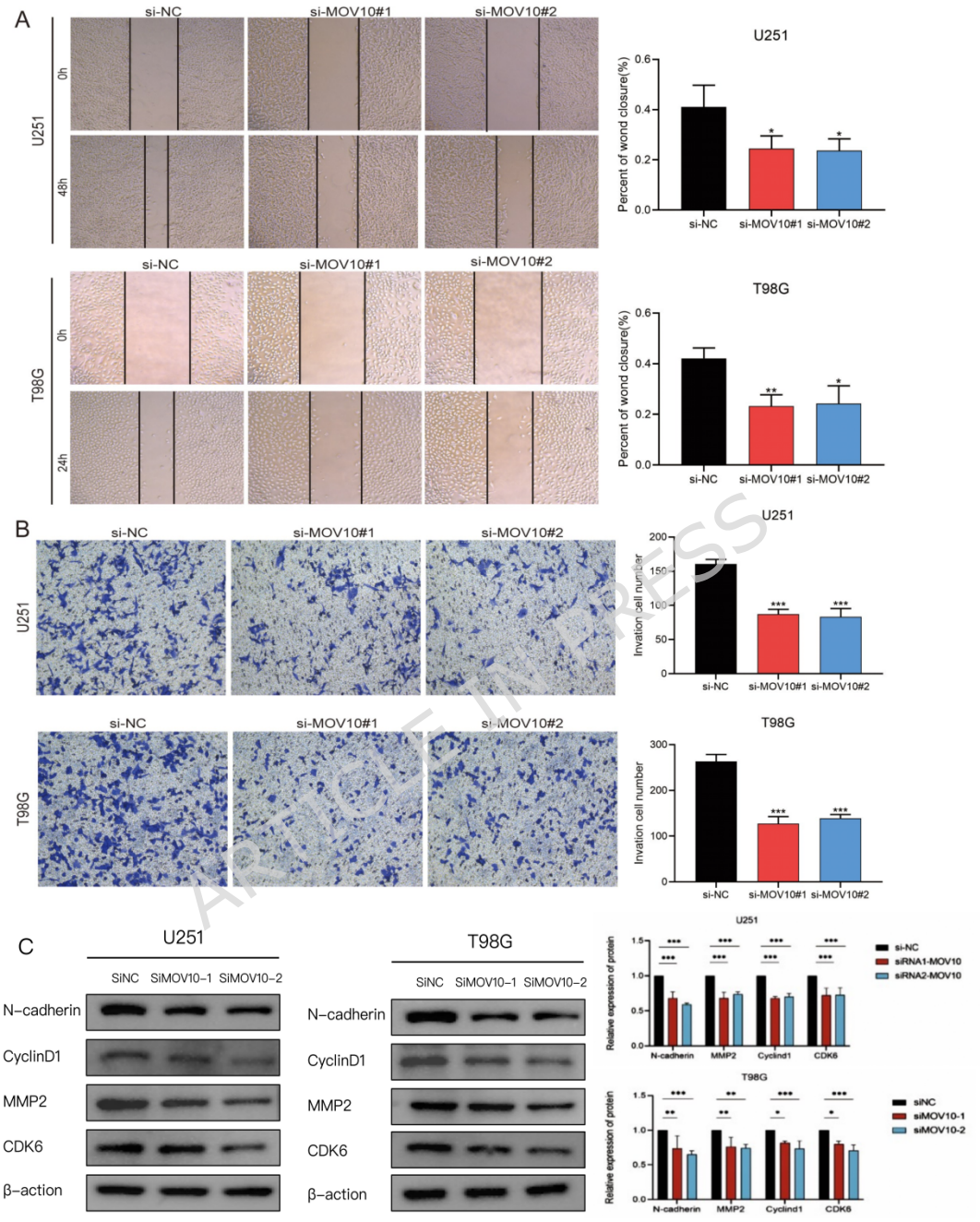

Figure 5: The depletion of MOV10 inhibited the migration and invasion of glioma cells by suppressing EMT. A: Wound-healing assays in T98G and U251 cells transfected with siMOV10. B: Transwell assays in T98G and U251 cells transfected with siMOV10. C: The protein expression levels of EMT- and proliferation-related proteins in T98G and U251 cells treated with MOV10

siRNAs (***p<0.001, **p<0.01, *p<0.05，n=3).

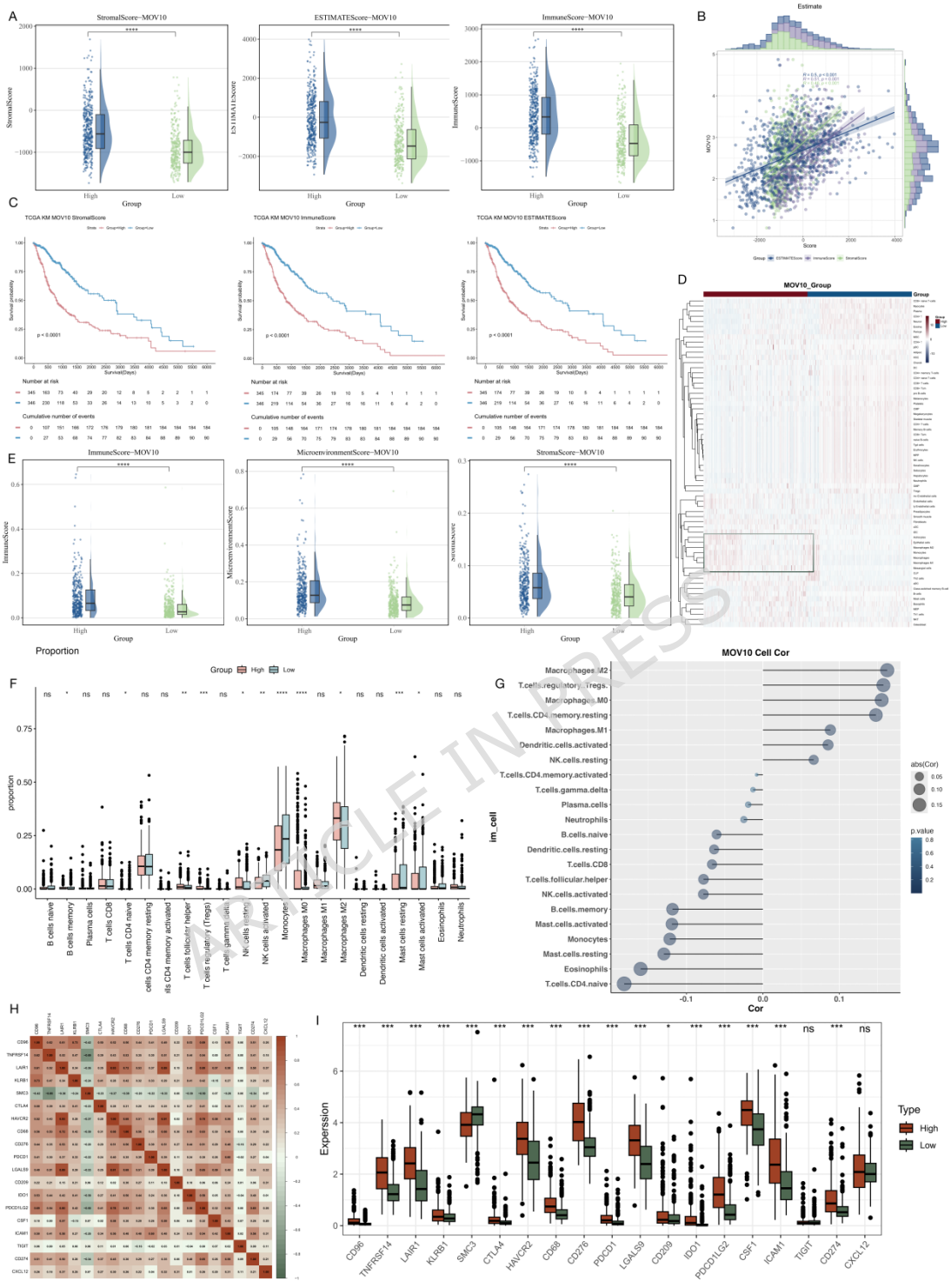

Figure 6: Immunological significance of MOV10 in glioma. A: ESTIMATE algorithm, tumor microenvironment (TME) scores comparing high MOV10 expression samples vs low expression samples. *p<0.05 vs low. B: Correlation analysis between MOV10 expression and TME scores using the ESTIMATE

algorithm. C: Overall survival (OS) curve comparing high and low stromal score groups (immune score) via the ESTIMATE algorithm. D: xCell algorithm, heatmap comparing cell expression between high and low MOV10 expression groups. E: xCell algorithm, TME scores for high vs low MOV10 expression samples. *p<0.05 vs low. F: Bar chart showing differences in various immune cell types between high and low MOV10 expression groups. G: Bubble chart demonstrating the correlation between MOV10 expression and 22 immune cell types in glioma. *p<0.05 vs low. H-I: Visualization of the differences and correlations between MOV10 expression and immune checkpoints in the TCGA-glioma dataset. *p<0.05 vs low. (***p<0.001, **p<0.01, *p<0.05).

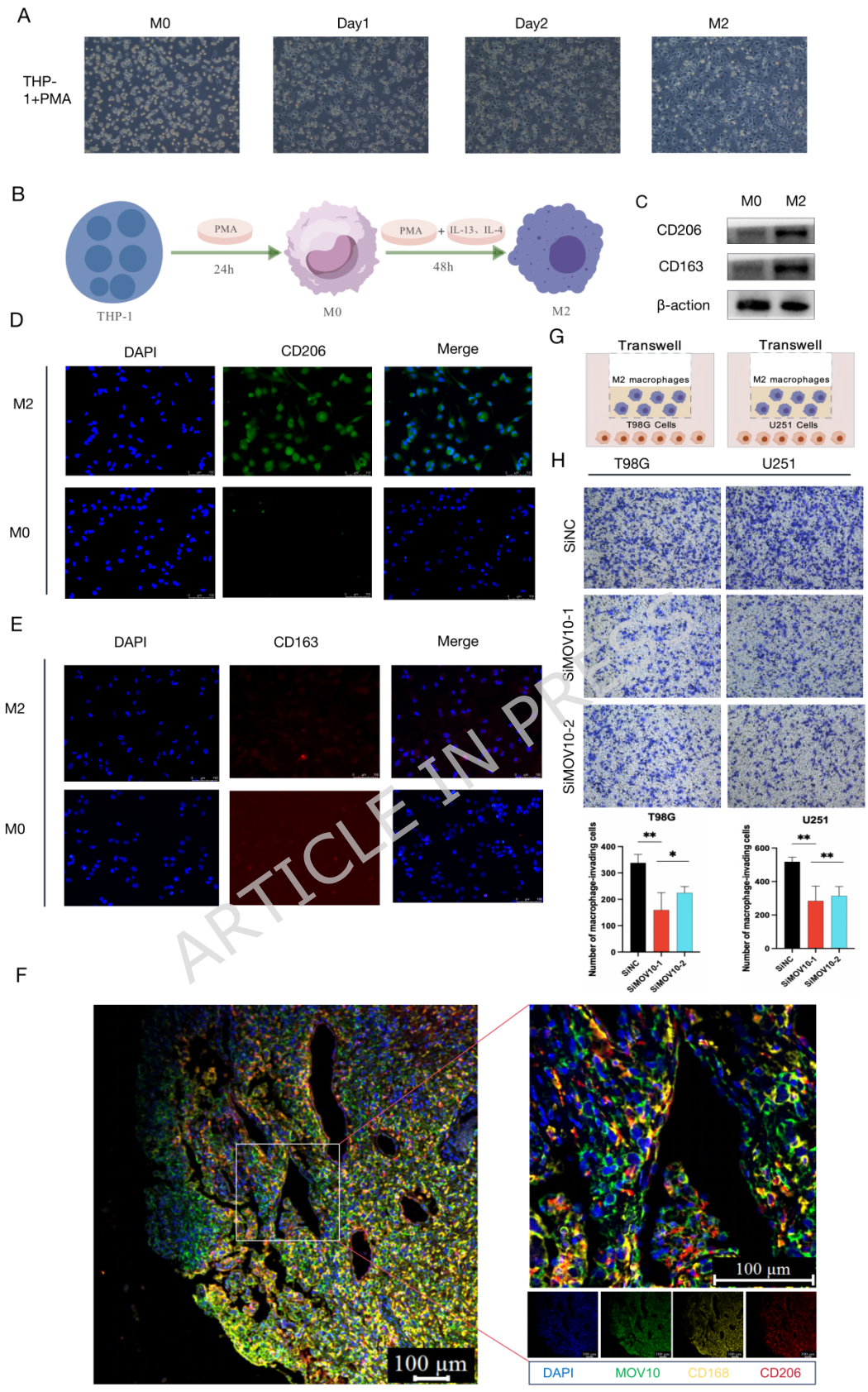

Fig. 7 Changes in macrophage migration after MOV10 deficiency. A: Polarization of THP-1 cells into M2 cells. B: M0-M2 model of THP-1 cells. C:

Western blot detection of the expression of M2 markers CD163 and CD206. D-E: Fluorescence analysis to detect the expression of CD163 and CD206 in M2 and M0 macrophages. F: The expression and co-localization of CD163, CD206 and MOV10 were detected in human glioma tissue using multiplex immunofluorescence analysis. G-H: Transwell analysis to examine the effect of MOV10 knockdown on the migration of U251 and T98G cells after co-culture with THP-1 cells and M2 macrophages for 48 hours (***$p<0.001$, **$p<0.01$, *$p<0.05$).

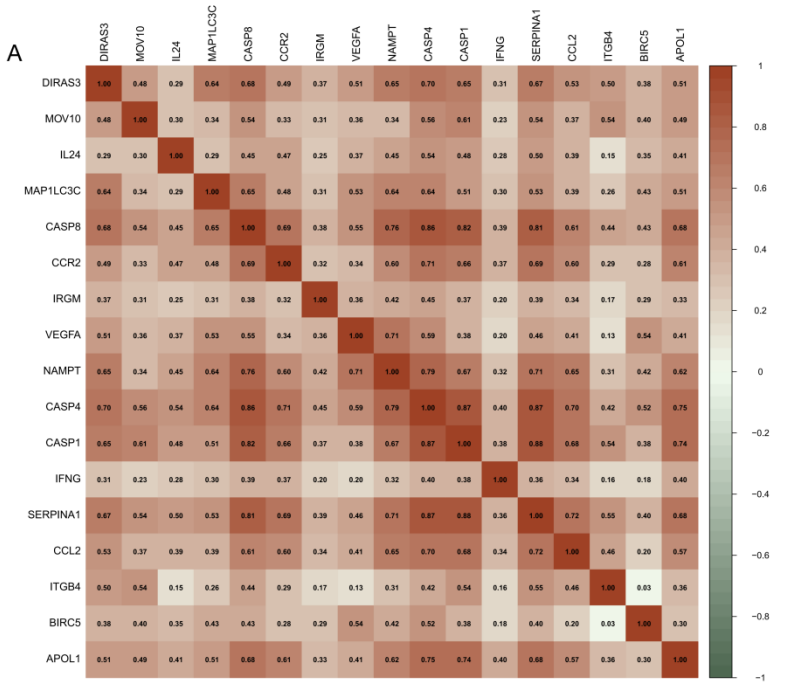

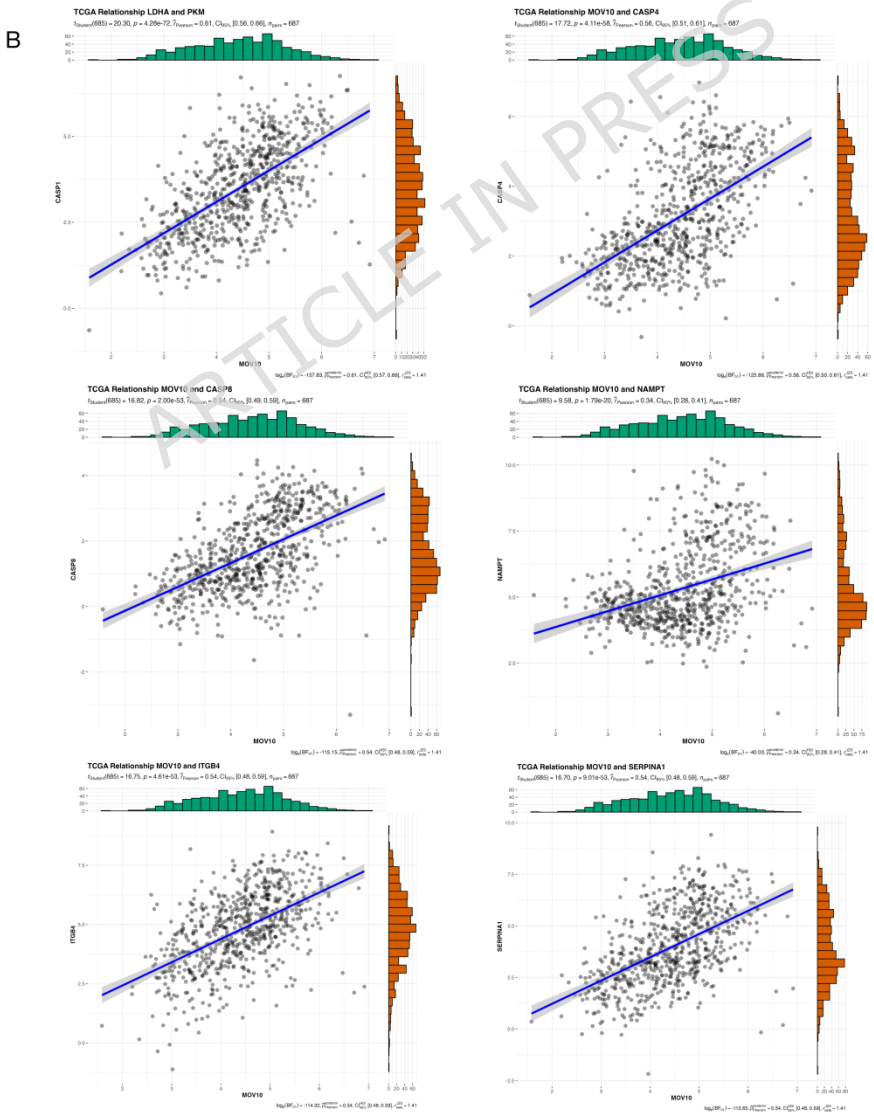

Figure 8: Association of MOV10 with autophagy in gliomas. A: Heatmap of the correlation of MOV10 with differentially expressed autophagy genes in the glioma expression matrix. B: Strong correlation of MOV10 with several differentially expressed autophagy genes, such as CASP1, CASP4, CASP8, ITGB4, NAMPT, and SERPINA1.

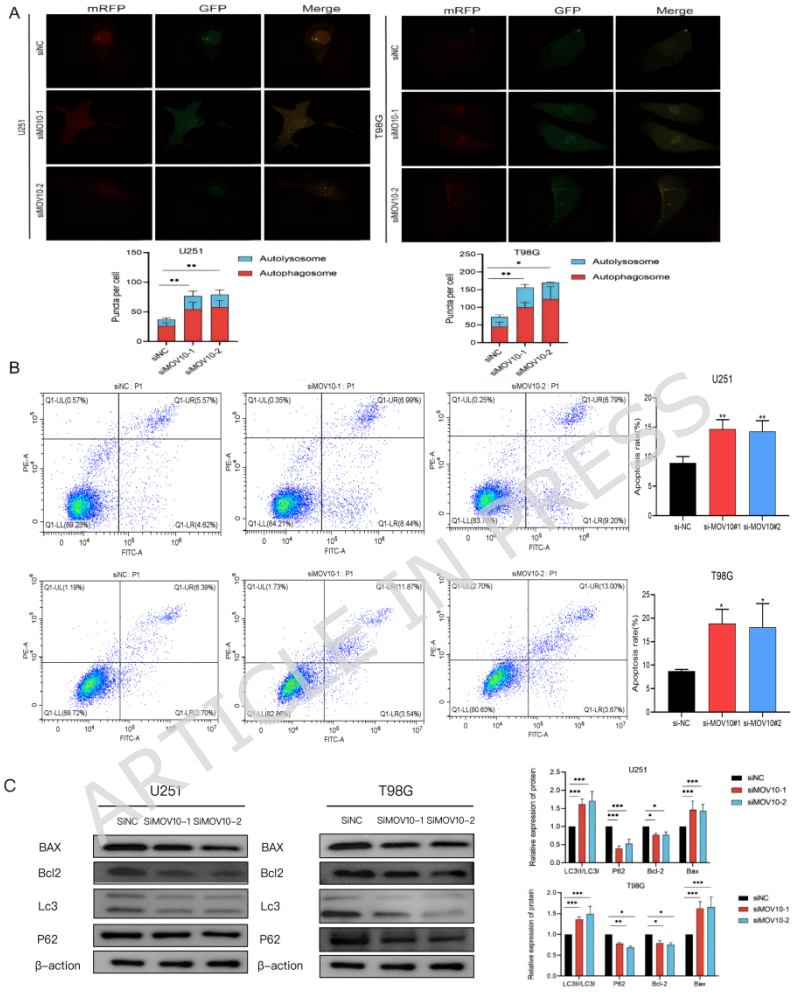

Figure 9: Knockdown of MOV10 promoted autophagy and apoptosis. A: The number of red and yellow puncta was elevated in glioma cells treated with MOV10 siRNAs. B: Apoptosis in T98G and U251 cells transfected with siMOV10 was detected by Annexin V and PI staining, respectively. C: The protein expression levels of autophagy- and apoptosis-related proteins in T98G and U251 cells treated with MOV10 siRNAs (***p<0.001, **p<0.01, *p<0.05，n=3).